Nucleation research progress for description of atmospheric aerosol dynamics.
2. Nucleation rate surface for water vapor

M. Anisimov, L. Anisimova,[1] P. Turner,[2] and Ph. Hopke[3]

Institute of Chemical Kinetics&Combustion,
Siberian Branch of the Russian Academy of Sciences, Novosibirsk, Russia
[1]Nucleation Laboratory, Institute of Catalysis,
Siberian Branch of the Russian Academy of Sciences, Novosibirsk, Russia
[2]Mathematics and Computer Science Department, Clarkson University, USA
[3]Department of Chemical Engineering, Clarkson University, USA

General computer algorithm for constructing the nucleation rate surface is developed. Algorithm is applicable in case of water vapor nucleation. Results can be used in calculations of the water vapor nucleation in atmosphere. An obvious advantage of the computer semi-empirical construction of nucleation rate surfaces is the ability to construct this surface over the whole interval of nucleation parameters that is impossible in experiments. Examples of hard-to-reach conditions include very low temperatures, media with high-pressures and/or very high-temperature (such as stars), etc. It is assumed that the current algorithm can be further developed for semi-empirical construction of nucleation rate surfaces for one- and two-component systems.

Introduction

During the past half-century, classical nucleation theory (CNT) has been developed, and there appear noticeable advances in the molecular theory of nucleation. Most efforts were directed towards modeling small molecule systems using intermolecular potentials. Summarizing the state of the nucleation theory, it can be concluded that it is far from complete. It is possible to successfully describe nucleation using sufficiently simple models of simple real systems.[1] However, up to now, experimental data and theory often disagree, and in the best cases, show their agreement only in narrow intervals of nucleation temperatures. The available nucleation data represent small islands in the total field of nucleation conditions: from the critical temperature to absolute zero. These basic limitations in data are a good reason to develop semi-empirical constructions of nucleation rate surfaces in order to interpolate and extrapolate the available experimental data to areas, for which the information is entirely absent.

We have worked out an algorithm for semi-empirical construction of nucleation rate surfaces. As an example of some unary system, the topology of the water vapor nucleation rate surface is discussed. Nucleation of two concurrent (stable and unstable) phases in the critical germs is considered in the context of multi-surface nucleation rates. For simplicity, only one phase transition (melting) is included in the considered states of water. Several plausible assumptions are used to construct the nucleation rate over the whole temperature interval from critical point to absolute zero.

Basic principles

Following the approach by Anisimov (Ref. 2), the nucleation rate surface for any system can be constructed based on its phase diagram. The concept involves the use of the phase equilibrium diagram as lines of zero nucleation rates. The nucleation rate surfaces arise from the equilibrium lines. Only limited amount of experimental data is needed in normalizing the slopes of the linearized nucleation rates. The nucleation rate surface is described in terms of steady-state nucleation rates. To construct the surfaces of nucleation rates, some assumptions from Ref. 3 are used. All of these assumptions are commonly used to describe the first order phase transitions. The main characteristic of nucleation (or phase transitions of the first order) is the ability to separate the initially homogeneous parent phase into two or more phases. This condition contradicts to characteristics of phase transition of the second order. The critical point or critical line (for binary system) represents the conditions for the second order phase transitions, under which coexistence of two or more phases is impossible.

Assuming that the nucleation rate is represented by a continuous, monotonic function, it can be stated that *the nucleation rate decreases when approaching a second order phase transition and becomes zero for a second order phase transition*. Systems cannot reach the conditions of the second order phase

transition because of the growing fluctuations near the phase transition in the initial phase. Therefore, it is only possible to discuss the phase transition limit. The algorithm for semi-empirical construction[4] of the nucleation rate surface can be described as follows.

(a) Obtain an extension of the available data for stable and unstable phase equilibria to critical and the absolute zero temperatures for the system of interest.

(b) Define the conditions corresponding to the highest rates of nucleation (maximum under spinodal conditions in the present research) and extrapolate them to absolute zero.

(c) Assume that the chosen function for the nucleation rate (for example, exponent) holds under all nucleation conditions.

(d) Linearize the experimental nucleation rates, using (c), for all channels.

(e) Estimate the nucleation rates under the spinodal conditions and at any low ($\log J = -10$ in our case) nucleation rate, using linear approximation of the experimental data.

(f) Approximate spinodal nucleation rates using known values of nucleation rates under spinodal conditions including zero values at critical and zero temperatures.

(g) Repeat the process (f) for some given low nucleation rate ($\log J = -10$ in this case).

(h) Calculate the nucleation rate surface with the use of linearized functions based on approximations (f) and (g).

Equilibrium and spinodal lines of water vapor

To use the algorithm, all the experimental data for equilibrium states of water vapor in the form of temperature dependences of the pressure P were taken from the Smithsonian Meteorological Tables[5] and extrapolated to zero temperature through equations: $\log P_{lqd} = 11.6644 - 2422.2995/T$ and $\log P_{sld} = 12.5709 - 2670.5623/T$ for liquid and solid phases, respectively (Figs. 1 and 2).
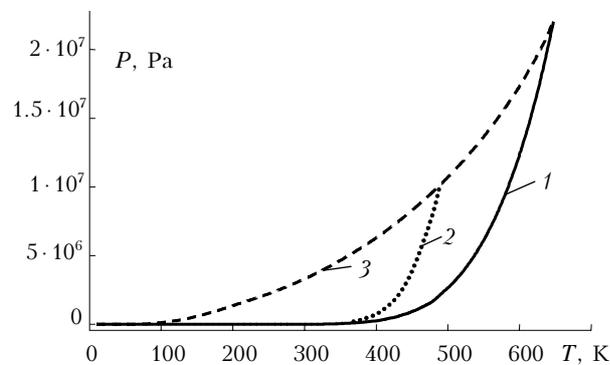
Fig. 1. The *PT* diagram for water: (*1*) the liquid-vapor equilibrium line; (*2*) the solid–vapor equilibrium line; (*3*) the spinodal line.

In these equations, the temperature T can vary from 0 to 220 K. Equilibrium lines include their extensions, which illustrate stable and unstable equilibria. The vapor–liquid, vapor–solid, and vapor spinodal lines are represented in Fig. 1 in all intervals of temperature and pressure. The vapor–ice equilibrium is extended to spinodal conditions (Fig. 2). The last (spinodal) point of this unstable equilibrium corresponds to a temperature of 487.2 K and a pressure of 10.00 MPa.
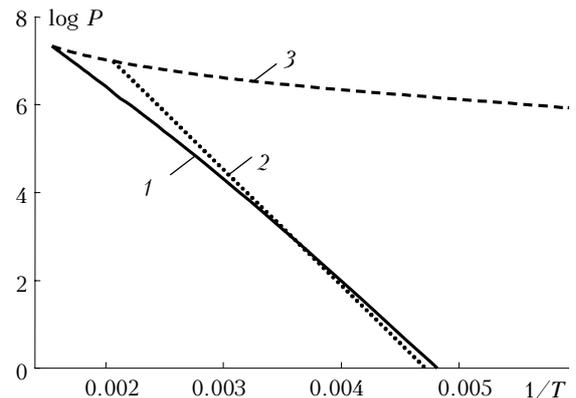
Fig. 2. Extrapolation conditions for the spinodal decomposition and phase equilibrium conditions (including the unstable one): (*1*) liquid–vapor equilibrium line; (*2*) solid–vapor equilibrium line; (*3*) spinodal line.

To calculate the spinodal conditions (pressure and temperature), we must use the equation of state. To find the nucleation rate topology at the absolute zero limit, it is necessary to extend the spinodal line to absolute zero representing the limit of the vapor existence. Spinodal conditions for water vapor were calculated using the Van der Waals equation of state

$$P = RT /(V - b) - aV^{-2} ,$$

where V is the volume; R is the gas constant; $a = 27(RT_c)^2/64P_c$ and $b = RT_c/8P_c$. The critical temperature $T_c = 647.3$ K and the critical pressure $P_c = 22.04832$ MPa for water were taken from Ref. 6. The spinodal conditions were extrapolated from 220 K to the absolute zero temperature using the equation: $\log P_{sp} = 7.2159 - 217.5720/T$.

Spinodal vapor supersaturation

Of particular interest is estimation of the vapor supersaturation for spinodal conditions over the whole temperature interval of the spinodal existence. Recently, it was suggested that the spinodal line for vapor metastable states tends to zero pressure at the zero temperature limit.[3] Consequently, the vapor supersaturation has an indeterminate value in the temperature zero limit. Figure 1 presents the spinodal lines for water vapor.

It seems that the spinodal vapor supersaturation should be equal to unity both at the absolute zero

limit and at the critical point. Unexpectedly, the vapor supersaturation value sharply increases with decreasing temperature; and the supersaturation logarithm reaches several hundreds at a few Kelvin degrees. In Fig. 3 the spinodal vapor supersaturation is shown only to 35 orders of magnitude.

Water vapor supersaturation under the spinodal condition grows dramatically from unity in the direction to zero temperature. Semi-empirical estimate of the vapor supersaturation under spinodal conditions can show if this result holds for other vapor.
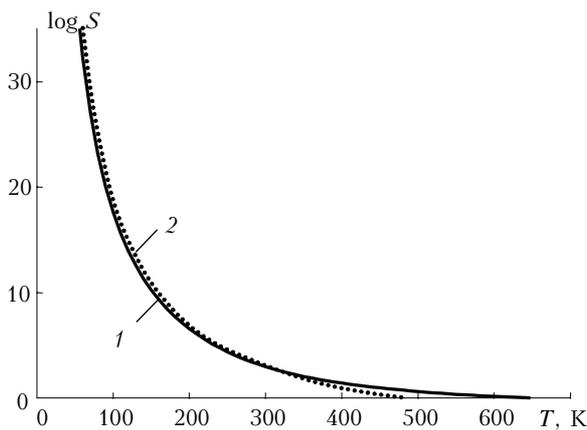

Fig. 3. Water vapor supersaturations under spinodal conditions: (*1*) vapor–liquid; (*2*) vapor–solid.

As it was mentioned above, the spinodal vapor pressure is assumed the same both for liquid and crystal formations. Therefore, the spinodal vapor supersaturation ratios are different for different phases because of the difference in the vapor equilibrium pressures over liquid and solid phases (Fig. 3). Seemingly, the water vapor supersaturation becomes infinite in the absolute zero limit or, more probably, supersaturation must be calculated in the quantum mechanics approximation. The vapor supersaturation growth (see Fig. 3) is clearly pronounced at $T = 350$ K, where estimate of the spinodal line vapor pressures is more accurate than at low temperatures.

Linearization of the nucleation data in each channel

It follows from Ref. 7 that vapor nucleation in the vicinity of its triple point is two-channel. In Ref. 8, the average frequencies of the appearance of supercooled water, mixed ice–droplet phase, and ice particles in clouds were experimentally determined. It has been found that water in atmospheric clouds can exist in the droplet or ice states simultaneously at temperatures of $230 - 270$ K (Ref. 8). It can be expected that particles keep initial phase state of their critical germs. It was noted in Ref. 9 that if air is saturated with respect to ice, it is subsaturated with respect to water. As a result, supercooled water

droplets cannot coexist in equilibrium with ice crystals. Continuing this idea, it can be said that ice decreases the amount of undersaturated vapor over droplets because of vapor pumping out through condensation (freezing). It decreases the size and the total number of droplet particles. Obviously, the mixture of droplets and ice particles in the atmosphere must be dynamic, because the processes of droplet freezing and vapor nucleating with formation of droplets and ice particles proceed there simultaneously.

The experimental data[10] correspond to nucleation temperatures below the triple point and they have to represent the resulting nucleation rate for water droplets and ice particles. The experimental data, taken by us from Ref. 10, have the rates not specified by the nature of the condensed phase.

Quantitative data on nucleation rates in each phase (liquid and ice) are not available. Therefore, we specified the phase states on the base of the reasonable topology, which is known for the triple point vicinity[2] for two nucleation channels. The intersection points for the ice and droplet nucleation rates are calculated using the published data[10] for total nucleation rate, i.e., joint values of ice and droplets. According to our estimates, the intersection line of surfaces of both phases is located within three orders of magnitude of the nucleation rate. It should be emphasized that the nucleation rate must be represented by two nucleation channels and two-sheet nucleation surface.

The nucleation rates for ice or liquid droplets can be described using the linearized approximation such as $\log J = a + b\log^{-2}S$, where J is the vapor nucleation rate, coefficients a and b are constant for given temperature T of nucleation. It is assumed that these approximations of the experimental nucleation rates are true for all nucleation conditions from zero to maximum value. The nucleation rates for ice J_s and droplets J_d (Fig. 4) can be described using the linear approximations from Table 1, where S is the vapor supersaturation ratio for the given phase, and T is the nucleation temperature. It is assumed that these approximations of the nucleation rates for each channel, listed in Table 1, hold for all nucleation conditions from zero to maximum value.

Table 1. Approximations of the quasiexperimental ice (J_s) and droplet (J_d) nucleation rates extracted from the experimental data[10] for nucleation temperatures, T(K)

T, K	$\log J_s$	$\log J_d$
220	$20.0357 - 21.6108\log^{-2}S$	$19.0615 - 14.1080\log^{-2}S$
230	$21.1240 - 19.1413\log^{-2}S$	$20.8838 - 13.5074\log^{-2}S$
240	$21.1723 - 15.6712\log^{-2}S$	$22.6646 - 12.9738\log^{-2}S$
250	$20.9976 - 12.8425\log^{-2}S$	$22.5084 - 11.2466\log^{-2}S$
260	$20.3089 - 9.9781\log^{-2}S$	$22.0372 - 9.6404\log^{-2}S$

The above point of view can be illustrated schematically by Fig. 5, where the linearized nucleation rate isotherm arises from the point of phase equilibrium.
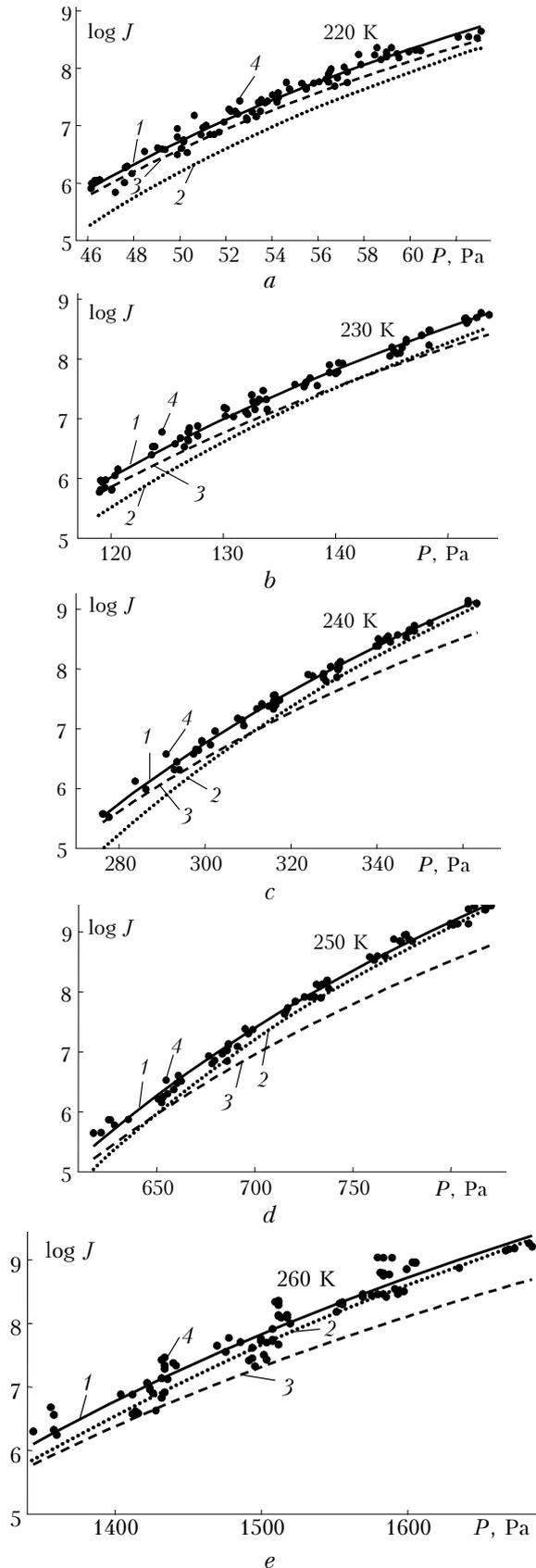
Fig. 4. Experimental data[10] (*4*) and their regressions (*1*) for the total nucleation rate for ice (*3*) and water droplets (*2*). Temperatures of nucleation are shown near each curve.

The slope of the linearization is defined by the experimental data points. The top point of linearization corresponds to the vapor spinodal conditions.
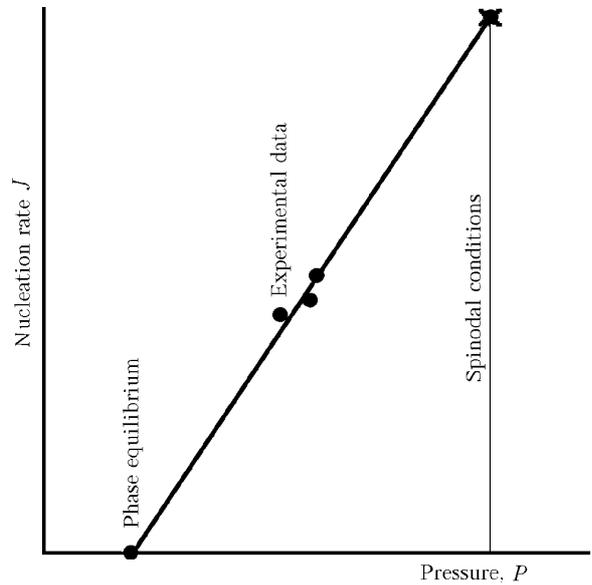
Fig. 5. Scheme of algorithm for the computer semi-empirical construction of nucleation rate surfaces.

Nucleation rate under spinodal conditions and the vapor supersaturation profile at $J = 10^{-10}\,\text{cm}^{-3}\text{s}^{-1}$

Extreme nucleation rates can be extrapolated to conditions of spinodal decomposition, which will result in estimates of nucleation rates under spinodal conditions. Zero rates of nucleation at the critical temperature and absolute zero as well as the extrapolated points provide for all currently available information on nucleation rate estimation under spinodal conditions. Possible spinodal nucleation rates are illustrated in Fig. 6 for the case of water vapor nucleation. Second order regression in the log J–T space is used to approximate the points for ice (black dots) and droplets (gray dots) using zero values of nucleation rates at the critical point and the absolute zero temperature limit. The regressions involve the equilibrium conditions as zero values of the nucleation rate. Nucleation rate of $10^{-10}\,\text{cm}^{-3}\cdot\text{s}^{-1}$ is used as a reference level in our consideration. Extrapolation of the linearized experimental data was used to estimate the supersaturation values for that nucleation rate.

Spinodal supersaturations and the supersaturations (or vapor pressures), estimated at the reference nucleation rate using the regressions for each phase nucleation rate (Fig. 4 and Table 1), can be used to depict the vapor pressure (bold line in Fig. 6) for the reference nucleation rate level. Figure 6 illustrates relative configurations of the spinodal nucleation rates for ice particles and water droplets, as well as the vapor pressure at $J = 10^{-10}\,\text{cm}^{-3}\cdot\text{s}^{-1}$.
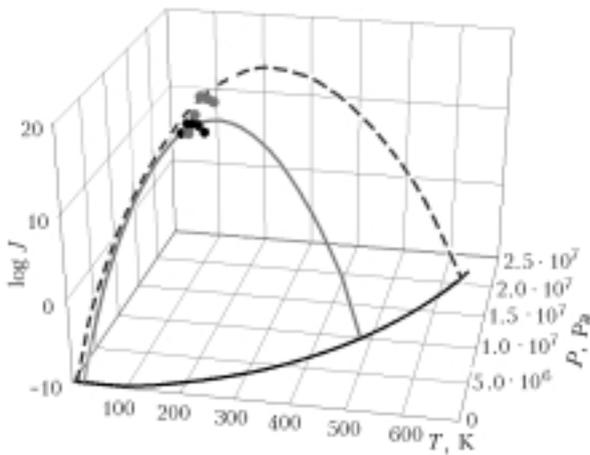
Fig. 6. Spinodal nucleation rates. Ice nucleation (gray line); droplet nucleation (dashed line); and vapor pressure (bold line).

Nucleation rate surface

The lowest level of nucleation rate surface at $J = 10^{-10}$ cm^{-3}·s^{-1} is low enough for any practical use because the nucleation rate $J = 10^{-10}$ cm^{-3}·s^{-1} yields only one nucleation event per cm^3 for more than 300 years. With linear approximation of the same kind (using scale or any other functional relations) for the given nucleation temperature ($\log J = a + b \, \log^{-2} S$ in our case), it is possible to build the nucleation rate surfaces for formation rates of any phase (crystal or liquid in our case). Insignificant extensions to the critical and absolute zero temperatures aiming at obtaining the total nucleation rate surface can be performed using any

reasonable extrapolation of constants, which were employed in linearization. Figure 7 illustrates the nucleation rate surface in the $\log J - T - P$ space. The alternative $J - T - P$ presentation is shown in Fig. 8. The equations representing the isotherms of the nucleation rate surfaces are collected in Table 2. The available experimental data on nucleation and equations of states play key roles in this semi-empirical construction.
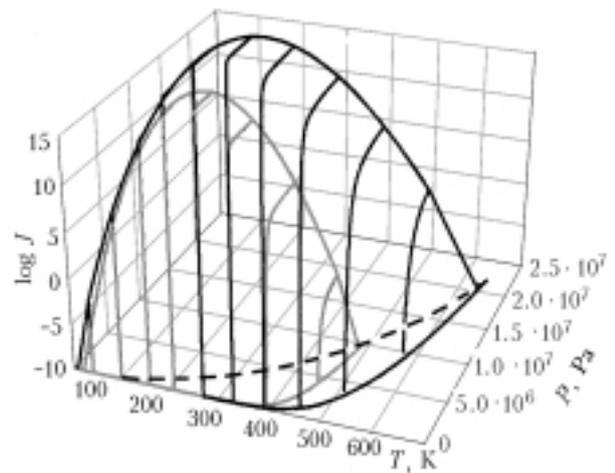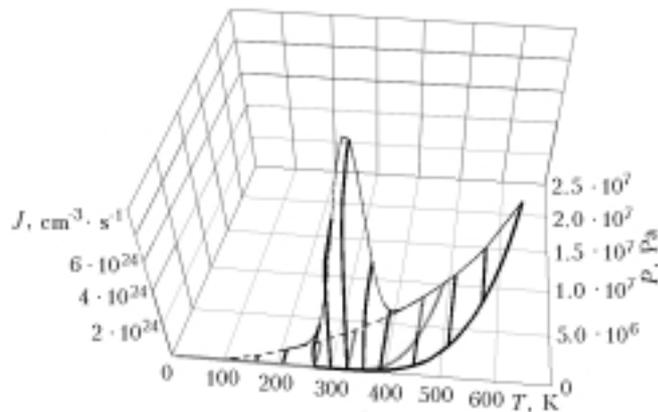

Fig. 7. Nucleation rate surfaces for water droplets and ice particles in the $\log J - P - T$ space; water droplet nucleation (bold lines); ice particle nucleation (gray lines); and vapor spinodal (dashed line).

Note that nucleation is considered here in the one-component approximation for the "water vapor — carrier gas" system. However, such nucleation in fact is binary, because the carrier gas takes part as the second component.[11]

Table 2. Equations representing the isotherms of the nucleation rate surfaces

For nucleation of droplets or glassy particles	For nucleation of solid phase (ice)
$\log J_d$ [20 K] $= -5.8046 - 12.3370\log^{-2}S$	$\log J_s$ [20 K] $= -9.9994 - (6.619\mathrm{e}{-3})\log^{-2}S$
$\log J_d$ [40 K] $= -1.8765 - 6.1199\log^{-2}S$	$\log J_s$ [40 K] $= -5.0543 - 12.2849\log^{-2}S$
$\log J_d$ [100 K] $= 8.3047 - 2.3702\log^{-2}S$	$\log J_s$ [100 K] $= 7.1300 - 6.0197\log^{-2}S$
$\log J_d$ [160 K] $= 16.0822 - 1.4137\log^{-2}S$	$\log J_s$ [160 K] $= 15.3388 - 3.0508\log^{-2}S$
$\log J_d$ [210 K] $= 20.7293 - 1.0224\log^{-2}S$	$\log J_s$ [210 K] $= 19.1441 - 1.8134\log^{-2}S$
$\log J_d$ [220 K] $= 21.4589 - 0.9643\log^{-2}S$	$\log J_s$ [220 K] $= 19.5742 - 1.6368\log^{-2}S$
$\log J_d$ [230 K] $= 22.1222 - 0.9107\log^{-2}S$	$\log J_s$ [230 K] $= 19.8940 - 1.4773\log^{-2}S$
$\log J_d$ [240 K] $= 22.7189 - 0.8613\log^{-2}S$	$\log J_s$ [240 K] $= 20.1037 - 1.3330\log^{-2}S$
$\log J_d$ [250 K] $= 23.2492 - 0.8154\log^{-2}S$	$\log J_s$ [250 K] $= 20.2031 - 1.2021\log^{-2}S$
$\log J_d$ [260 K] $= 23.7130 - 0.7726\log^{-2}S$	$\log J_s$ [260 K] $= 20.1923 - 1.0833\log^{-2}S$
$\log J_d$ [270 K] $= 24.1104 - 0.7327\log^{-2}S$	$\log J_s$ [270 K] $= 20.0714 - 0.9752\log^{-2}S$
$\log J_d$ [300 K] $= 24.9046 - 0.6269\log^{-2}S$	$\log J_s$ [300 K] $= 19.0483 - 0.7051\log^{-2}S$
$\log J_d$ [330 K] $= 25.1029 - 0.5376\log^{-2}S$	$\log J_s$ [330 K] $= 17.0365 - 0.4996\log^{-2}S$
$\log J_d$ [360 K] $= 24.7074 - 0.4606\log^{-2}S$	$\log J_s$ [360 K] $= 14.0399 - 0.3426\log^{-2}S$
$\log J_d$ [390 K] $= 23.7206 - 0.3930\log^{-2}S$	$\log J_s$ [390 K] $= 10.0676 - 0.2228\log^{-2}S$
$\log J_d$ [450 K] $= 19.9884 - 0.2785\log^{-2}S$	$\log J_s$ [450 K] $= -0.6056 - 0.0647\log^{-2}S$
$\log J_d$ [510 K] $= 14.0209 - 0.1840\log^{-2}S$	
$\log J_d$ [570 K] $= 6.2725 - 0.1055\log^{-2}S$	
$\log J_d$ [630 K] $= -12.5176 + 0.0141\log^{-2}S$	

Fig. 8. Alternative, $J–P–T$, pattern of the nucleation rate surfaces for water droplets and ice formation: ice particle nucleation (gray line); water droplet nucleation (solid bold line); spinodal nucleation for vapor nucleation (thin black line); and vapor spinodal (dash line).

Summary

The algorithm for computer semi-empirical construction of the nucleation rate surface for a single-component system with triple point is developed for the first time. The algorithm is realized for the case of water vapor nucleation rate surface. The nucleation rate surface is constructed for all conditions possible from physical point of view. An obvious advantage of the semi-empirical construction of nucleation rate surfaces is a possibility to construct this surface over the whole interval of variation of nucleation parameters, that is impossible experimentally. It is assumed that the algorithm will be further developed for the semi-empirical construction of nucleation rate surfaces for one- and two-component systems.

The construction of the nucleation rate surfaces for water has clarified additional requirements in studying nucleation, namely:

— nucleation rates must be measured in each channel of nucleation;

— additional theoretical study is needed to provide a better extrapolation or scaling of nucleation rates to spinodal conditions;

— theoretical validation is needed of classes of functions, which can be used in approximation of nucleation rates at a reference level of spinodal and low rates;

— experimental range of the nucleation rate measurements is very narrow in comparison with total range of the nucleation process.

Measurements should be optimized to provide for the critical reference points for the nucleation rate surface construction. Data collected in Table 2 can be used in practical calculation of nucleation of ice particles and droplets, which can proceed under atmospheric conditions. Obtaining of actual measurements of nucleation rates for each channel of nucleation may require a correction of the available data.

Acknowledgments

References

1. H. Reiss, in *Nucleation and Atmospheric Aerosols,* ed. by B. Hale and M. Kulmala (AIP, Melville, NY, 2000), p. 181.
2. M.P. Anisimov, J. Aerosol Sci. **21**, Suppl. 1, 23–26 (1990).
3. M.P. Anisimov,   P.K. Hopke,   D.H. Rasmussen, S.D. Shandakov, and V.A. Pinaev, J. Chem. Phys. **109**, No. 4, 1435–1444 (1998).
4. M. Anisimov, L. Anisimova, P. Turner, and P. Hopke, in: *Proc. of 16th International Conference on Nucleation and Atmospheric Aerosols*, (Kyoto University Press, Kyoto, 2004), pp. 205–209.
5. *Smithsonian   Meteorological   Tables*   (Smithsonian Institution Press, Washington, 1968), Vol. 114, p. 453.
6. D.R. Lide, ed., *Handbook of Chemistry and Physics*, 76th edition (CRC Press, Boca Raton, New York–London–Tokyo, 1995–1996).
7. L. Anisimova, P.K. Hopke, and J. Terry, J. Chem. Phys. **114**, No. 20, 9852–9856 (2002).
8. A.M. Boronikov,   L.I. Gaivoronskii,   E.G. Zak, V.V. Kostarev, I.P. Mazin, M.E. Minervin, A.K. Khrgian, and S.M. Shmeters, *Cloud Physics*, Israel Program for Scientific Translations, Jerusalem, Israel (1963).
9. J.H. Seinfeld and   S.N. Pandis,   in: *Atmospheric Chemistry and Physics* (J. Wiley&Sons, Inc., New York, 1998), p. 1326.
10. Y. Viisanen, R. Strey, and H. Reiss, J. Chem. Phys. **112**, No. 18, 8205–8212 (2000).
11. M.P. Anisimov, J.A. Koropchak, A.G. Nasibulin, and L.V. Timoshina, J. Chem. Phys. **109**, No. 22, 10004–10010 (1998).